Stability of mixed convection in an anisotropic vertical porous channel

P. Bera, and A. Khalili

View Online   Export Citation

ARTICLES YOU MAY BE INTERESTED IN

Influence of Prandtl number on stability of mixed convective flow in a vertical channel filled with a porous medium
Physics of Fluids **18**, 124103 (2006); https://doi.org/10.1063/1.2405321

Weakly nonlinear stability analysis of non-isothermal Poiseuille flow in a vertical channel
Physics of Fluids **27**, 064103 (2015); https://doi.org/10.1063/1.4922342

Instability of mixed convection in a vertical porous channel with uniform wall heat flux
Physics of Fluids **25**, 084108 (2013); https://doi.org/10.1063/1.4819121
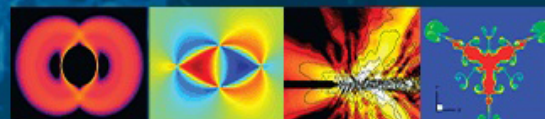
Stability of mixed convection in an anisotropic vertical porous channel

P. Bera and A. Khalili[a)]
Max Planck Institute for Marine Microbiology, 28359 Bremen, Germany

This paper addresses the stability of mixed convective buoyancy assisted flow due to external pressure gradient and buoyancy force in a vertical fluid saturated porous channel with linearly varying wall temperature. The porous medium is assumed to be both hydrodynamically and thermally anisotropic. Two different types of temperature perturbations, (i) zero temperature and (ii) zero heat flux, have been considered to study the effect of anisotropic permeability and thermal diffusivity on the flow stability. The stability analysis indicated that the least stable mode is two-dimensional. Furthermore, the results show that for the same Reynolds number, the fully developed base flow is highly unstable (stable) for high (low) permeable porous media as well as for a porous medium with small (large) thermal diffusivity ratio. Depending on the magnitude of all parameters studied, three types of instabilities (shear, thermal, and mixed instability) occurred. The transition of instability from one type to another took place smoothly, except when the permeability ratio exceeded 6. Based on the value of the permeability ratio, the flow in an anisotropic medium for a specific Reynolds number may be either more or less stable than the flow in an isotropic medium. In addition, the fully developed flow is more stable for relatively small values of the modified Darcy number than for larger values. The effect of Brinkman as well as Forchheimer terms are negligible for the set of other parameters studied here. In contrast to a pure viscous fluid or an isotropic porous medium, which are characterized by unicellular convective cells, in anisotropic porous media convective cells may be unicellular or bicellular. The stability analysis of mixed convection in channels filled either with a viscous fluid or with an isotropic saturated porous medium may be obtained as special cases of the general study presented here. © *2002 American Institute of Physics.* [DOI: 10.1063/1.1460879]

I. INTRODUCTION

In recent years, much work has been dedicated to the area of convective heat transfer in porous media because of its relevance to a variety of situations occurring in engineering and nature. Among these works, natural and forced convection studies occupy the majority of investigations. The interfacial area of mixed convection which connects natural and forced convection, in comparison, has not been given due attention in porous media. Mixed convection problems in porous media occur very often in nature, e.g., in studies of shallow-water and deep-sea hydrodynamics. One important example of mixed convection in shallow-water seas is given by hydrothermal vents by which hot, mineral-rich water ejects through a permeable seabed.[1–3] This problem constitutes a very new research area, and theoretical investigation of it has been largely overlooked. For fluid environments, however, there are many papers which deal with mixed convection, for example, in connection with fluid flow in a vertical pipe (Scheele and Hanratty,[4] Kemeny and Somers,[5] Yao,[6,7] Su and Chung[8]), in a vertical annulus (Yao and Rogers[9]), and in a vertical channel (Suslov and Paolucci,[10] Chen and Chung[11]).

Few investigations of mixed convection through a porous medium have been reported by Combarnous and Bia[12] on the effect of flow on the onset of convection, and by Cheng, who investigated in several studies the effect of mixed convection about inclined surfaces,[13] about a horizontal flat plate embedded in a porous medium with aiding external flow and constant heat flux,[14] and about a horizontal surface with a heat flux.[15] For the same geometry, Lai and Kulacki,[16] Renken and Paulikakos[17] have given an estimation of the boundary layer thickness via similarity solution and experiments, respectively.

More recently, Prasad *et al.*[18] studied a horizontal porous layer heated from below and investigated numerically the conditions for forced flow and buoyant effects for a wide range of Rayleigh and Peclet numbers. Most of the investigations considering the effect of anisotropy have been carried out for the onset of natural convection in horizontal porous layers. For example, Castinel and Combarnous[19] derived the criterion for the stability of a porous medium which is anisotropic in permeability. The same was given by Ephere[20] when the diffusivity is regarded as anisotropic, and in a combined form of anisotropic permeability and thermal diffusivity by Khalili *et al.*[21] Later, Tyvand[22] accounted for the effect of hydrodynamic dispersion caused by a uniform basic flow. The onset of convection as well as slightly supercritical convection through anisotropic multilayered porous media were investigated by McKibbin and Tyvand.[23] The onset of Rayleigh–Bénard convection in a horizontal porous

---

a)Author to whom correspondence should be addressed; electronic mail: akhalili@mpi-bremen.de
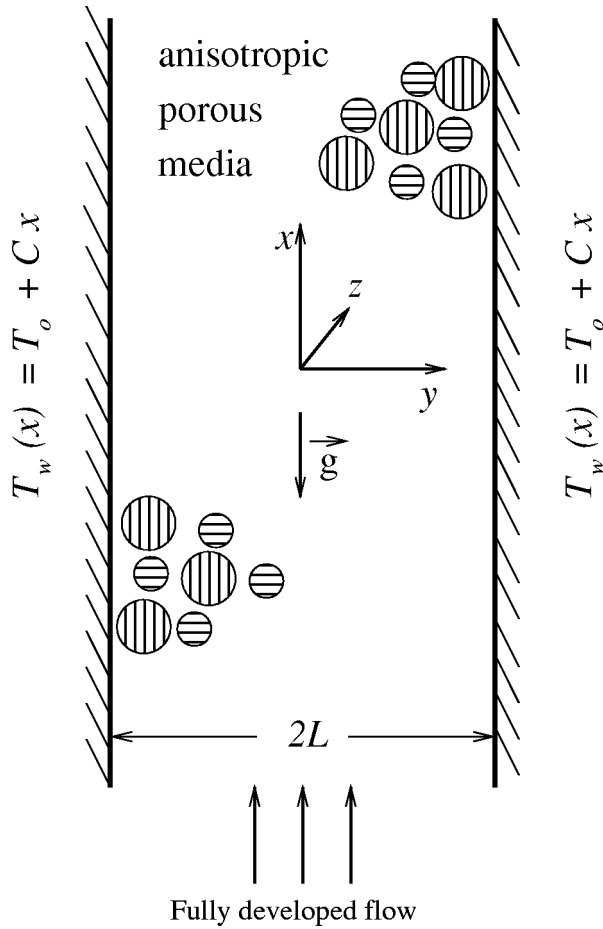
FIG. 1. Schematic of the problem considered.

layer with anisotropic permeability was investigated by Tyvand and Storesletten.[24] These works have not yet been extended to vertical porous geometries.

The present paper is concerned with studying the effect of anisotropy in permeability and thermal diffusivity on the stability of mixed convection in a vertical channel filled with a porous medium. Because the response of the stability of the system depends on the nature of the boundary condition, two types of boundary conditions, namely constant temperature as well as constant heat flux, are maintained at the bounding vertical channel walls. An outline of the paper is as follows: the mathematical formulation is given in Sec. II, which contains details of the stability analysis starting from the equations for the basic state, the perturbed equations, and their solution followed by the energy analysis. Section III discusses the effect of different anisotropic parameters on the stability of the fluid flow and heat transfer. Finally, some important features of the analysis are summarized in Sec. IV.

II. MATHEMATICAL FORMULATION

We consider a fully developed mixed convection flow caused by an external pressure gradient and a buoyancy force in a vertical porous channel of width $2L$ (see Fig. 1). The wall temperature (T_w) is linearly varying with x as $T_w = T_0 + Cx$, where C is a positive constant and T_0 is the upstream reference wall temperature. The gravitational force is aligned

in the negative x direction. The thermophysical properties of the fluid are assumed to be constant except for density dependency of the buoyancy term in the momentum equations. The porous medium is saturated with a fluid that is in local thermodynamic equilibrium with the solid matrix. The medium is anisotropic in permeability and thermal diffusivity. The longitudinal and transverse components of the permeability as well as thermal diffusivity are denoted by K_x, K_y and k_x, k_y, respectively. In expressing the equation for the flow in the porous medium, it should be noted that the Darcy model presents a linear relationship between velocity of discharge and the pressure gradient. As the Darcy model does not hold when the flow velocity is not sufficiently small, or when the permeability is high, extensions to this model known as Brinkman-extended or Forchheimer-extended models exist.[25,26] In short, the Brinkman term is found to be needed for satisfying a no-slip boundary condition at solid walls, whereas the Forchheimer term accounts for the form drag. Also in analogy with the Navier–Stokes equations, the Darcy model has been extended by including the material derivative.[27] The necessity of the simultaneous inclusion of all or some of these extensions has been discussed in the literature.[28–35] Therefore, in order to cover extreme values of input parameters (i.e., high permeability, high velocity, and low thermal diffusivity), the governing equations for the flow and heat transfer in Cartesian coordinate system (y,x,z) are given by

$$\nabla \cdot \mathbf{V} = 0, \tag{1}$$

$$\rho_f \left[\frac{1}{\varepsilon} \frac{\partial \mathbf{V}}{\partial t} + \frac{1}{\varepsilon^2} \mathbf{V} \cdot \nabla \mathbf{V} + \frac{c_F}{\|\bar{\bar{K}}\|^{1/2}} |\mathbf{V}| \mathbf{V} \right]$$
$$= -\nabla P + \rho \mathbf{g} + \tilde{\mu} \nabla^2 \mathbf{V} - \mu_f \frac{\mathbf{V}}{\bar{\bar{K}}}, \tag{2}$$

$$\sigma \frac{\partial T}{\partial t} + \mathbf{V} \cdot \nabla T - \nabla \cdot \bar{\bar{k}} \cdot \nabla T = 0, \tag{3}$$

$$\rho = \rho_f \{1 - \beta_T (T - T_w)\} \tag{4}$$

with $\bar{\bar{K}}$ and $\bar{\bar{k}}$ being the second-order permeability and thermal diffusivity tensors, respectively, given by

$$\bar{\bar{K}} = \begin{bmatrix} K_y & 0 & 0 \\ 0 & K_x & 0 \\ 0 & 0 & K_z \end{bmatrix}, \quad \bar{\bar{k}} = \begin{bmatrix} k_y & 0 & 0 \\ 0 & k_x & 0 \\ 0 & 0 & k_z \end{bmatrix}.$$

In the above equations, $\mathbf{V}(v,u,w)$, P, T, and ρ_f are the flow velocity, pressure, temperature and fluid density, respectively. Further, $\mathbf{g}$, ε, c_F, $\tilde{\mu}$, μ_f, β_T, and $\sigma = (\rho c)_m / (\rho c_P)_f$ are the gravitational acceleration, porosity, form drag coefficient, effective viscosity, fluid viscosity, volumetric thermal expansion coefficient, and ratio of heat capacities, respectively. The variable c denotes the specific heat, and the subscripts m and f stand for porous "medium" and "fluid," respectively.

Using nondimensional quantities $x^* = x/L$, $P^* = PL^2 / \rho_f \tilde{\nu}^2$, $t^* = t \tilde{\nu} P_g / L^2$, $\mathbf{V}^* = \mathbf{V} L / \tilde{\nu} P_g$, $\Theta = (T - T_w) / CL \, \mathrm{Pr}^* P_g$, Eqs. (1)–(4) become (asterisks neglected)
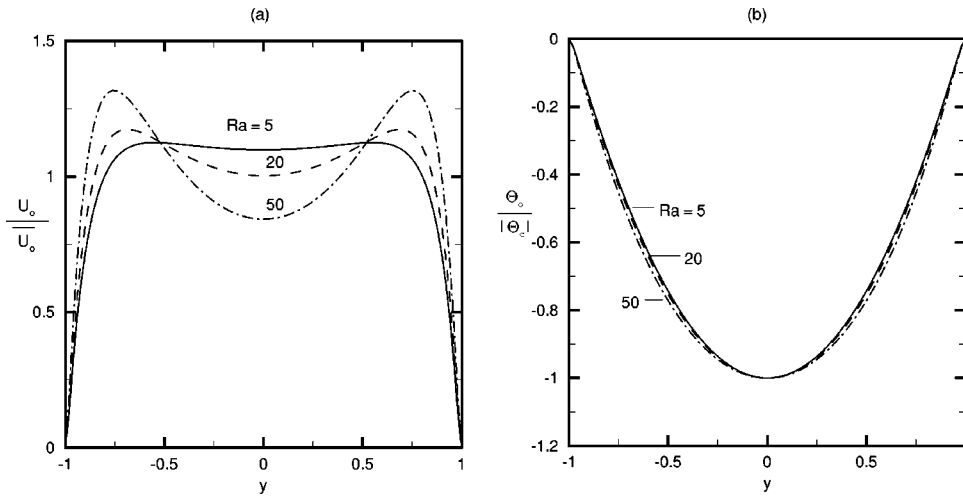
FIG. 2. Velocity profile (a) and temperature field (b) of the basic state for $K_1=0.1$, $k_1=0.2$, $Da^*=10^{-2}$, $F=1$.

$$\nabla \cdot \mathbf{V} = 0, \tag{5}$$

$$\frac{P_g}{\varepsilon}\frac{\partial \mathbf{V}}{\partial t} + \frac{P_g}{\varepsilon^2}(\mathbf{V}\cdot\nabla)\mathbf{V}$$

$$= -\frac{1}{P_g}\nabla P - \frac{\bar{\bar{M}}}{Da^*}\mathbf{V} - \frac{F}{K_0}|\mathbf{V}|\mathbf{V} + Ra\,\Theta\,\vec{e}_x + \nabla^2\mathbf{V}, \tag{6}$$

$$\sigma\frac{\partial \Theta}{\partial t} + u\frac{\partial \Theta}{\partial x} + v\frac{\partial \Theta}{\partial y} + w\frac{\partial \Theta}{\partial z}$$

$$= \frac{1}{P_g\,Pr^*}\left(\frac{\partial^2\Theta}{\partial x^2} + k_1\frac{\partial^2\Theta}{\partial y^2} + k_2\frac{\partial^2\Theta}{\partial z^2} - u\right), \tag{7}$$

where $P_g = -dP/dx$ is the pressure gradient, $Da^* = \bar{\mu}K_x/\mu_f L^2$ is the modified Darcy number, $F = c_F L P_g / K_x^{1/2}$ is the Forchheimer number, $Ra = g\beta_T C L^4/\tilde{\nu}k_x$ is the Rayleigh number, $Pr^* = \tilde{\nu}/k_x$ is the modified Prandtl number, $\tilde{\nu}$ is the effective kinematic viscosity, $k_1 = k_y/k_x$ and $k_2 = k_z/k_x$ are thermal diffusivity ratios. Further, the parameter K_0 is given by

$$K_0 = \frac{\|\bar{\bar{K}}\|^{1/2}}{K_x^{1/2}}$$

and

$$\bar{\bar{M}} = \begin{bmatrix} K_1 & 0 & 0 \\ 0 & 1 & 0 \\ 0 & 0 & K_2 \end{bmatrix}$$

is the modified permeability tensor, where

$$K_1 = K_x/K_y, \quad K_2 = K_x/K_z.$$

For the quantity $\|\bar{\bar{K}}\|^{1/2}$, the infinity norm defined by

$$\|\bar{\bar{K}}\| = \max_i \sum_{j=1}^{3} |K_{ij}|$$

is taken.

A. Basic state

The basic state is a fully developed, unidirectional, steady, and laminar flow. Under this circumstance the governing equations (5)–(7) are reduced to

$$1 - \frac{1}{Da^*}U_0 - \frac{F}{K_0}|U_0|U_0 + Ra\,\Theta_0 + \frac{d^2U_0}{dy^2} = 0, \tag{8}$$

$$U_0 = k_1\frac{d^2\Theta_0}{dy^2}, \tag{9}$$

with U_0 and Θ_0 being the base velocity and base temperature. The associated boundary conditions for velocity and temperature are $U_0 = \Theta_0 = 0$ at $y = \pm 1$. With these conditions, (8) and (9) can be solved numerically, using finite differences. Typical basic velocity and temperature profiles normalized by mean velocity $\bar{U}_0$ and Θ_c (i.e., Θ_0 at $y=0$), respectively, are given in Figs. 2(a) and 2(b), respectively, for different Raleigh numbers. As can be seen, the velocity profile for $Ra=20$, 50 with $k_1=0.2$, $Da^*=10^{-2}$, $F=1$ contains points of inflection which could give rise to instability.

B. Disturbance

Having calculated the basic state solution, its stability is investigated by means of linear theory.[36–38] Using infinitesimal disturbances on the fully developed laminar base flow, the solution of the three-dimensional problem can be written in the form

$$(\mathbf{V},P,\Theta) = (U_0(y)\vec{e}_x, P_0(x), \Theta_0(y)) + (\mathbf{V}',P',\Theta'). \tag{10}$$

The primed quantities denote the infinitesimal disturbances on the corresponding terms and can be represented by $(\mathbf{V}',P',\Theta')^T = e^{i(\alpha x + \beta z - \alpha ct)}(\hat{\mathbf{V}}, P(\hat{y}), \Theta(\hat{y}))^T$, with α and β being real-valued wave numbers in the x and z direction, respectively, and $c = \hat{c}_r + i\hat{c}_i$ the complex wave speed. The growth and decay of the disturbances depends on $\hat{c}_i$. Three different cases may be distinguished, i.e., stable, neutrally stable, or unstable depending on whether $\hat{c}_i < 0$, $\hat{c}_i = 0$, or $\hat{c}_i > 0$, respectively. Upon substitution of (10) into (5)–(7) and eliminating the pressure, the governing linear equations for the infinitesimal disturbances may be written as

$$\frac{d^4\hat{v}}{dy^4} - 2(\alpha^2+\beta^2)\frac{d^2\hat{v}}{dy^2} + (\alpha^2+\beta^2)^2\hat{v} + i\alpha\frac{P_g}{\varepsilon^2}\left[-U_0\frac{d^2\hat{v}}{dy^2} + \frac{d^2U_0}{dy^2}\hat{v} + (\alpha^2+\beta^2)U_0\hat{v}\right]$$

$$+ \frac{1}{Da^*}\left[-\frac{K_2\beta^2+\alpha^2}{(\alpha^2+\beta^2)}\frac{d^2\hat{v}}{dy^2} + K_1(\alpha^2+\beta^2)\hat{v} - \frac{i\alpha\beta(K_2-1)}{(\alpha^2+\beta^2)}\frac{d\hat{\eta}}{dy}\right] - \left(\frac{\alpha^2}{(\alpha^2+\beta^2)}+1\right)F_m\frac{d}{dy}\left(|U_0|\frac{d\hat{v}}{dy}\right) + (\alpha^2+\beta^2)F_m|U_0|\hat{v}$$

$$+ \frac{i\alpha\beta}{(\alpha^2+\beta^2)}F_m\frac{d}{dy}(|U_0|\hat{\eta}) - i\alpha\,Ra\frac{d\hat{\Theta}}{dy} = i\alpha c\frac{P_g}{\varepsilon}\left[-\frac{d^2\hat{v}}{dy^2} + (\alpha^2+\beta^2)\hat{v}\right], \tag{11}$$

$$-\frac{d^2\hat{\eta}}{dy^2} + (\alpha^2+\beta^2)\hat{\eta} + i\alpha\frac{P_g}{\varepsilon^2}U_0\hat{\eta} + \beta\frac{P_g}{\varepsilon^2}\frac{dU_0}{dy}\hat{v} - \beta\,Ra\,\hat{\Theta} + \frac{1}{Da^*}\left[\left(\frac{\beta^2+K_2\alpha^2}{(\alpha^2+\beta^2)}\right)\hat{\eta} + \frac{i\alpha\beta}{(\alpha^2+\beta^2)}(1-K_2)\frac{d\hat{v}}{dy}\right]$$

$$+ \left(\frac{\beta^2}{(\alpha^2+\beta^2)}+1\right)F_m|U_0|\hat{\eta} + \frac{i\alpha\beta}{(\alpha^2+\beta^2)}F_m|U_o|\frac{d\hat{v}}{dy} = i\alpha c\frac{P_g}{\varepsilon}\hat{\eta}, \tag{12}$$

$$\frac{1}{P_g\,Pr^*}\left[-k_1\frac{d^2\hat{\Theta}}{dy^2} + (\alpha^2+k_2\beta^2)\hat{\Theta}\right] + i\alpha U_0\hat{\Theta} + \frac{d\Theta_0}{dy}\hat{v} + \frac{1}{P_g\,Pr^*(\alpha^2+\beta^2)}\left(i\alpha\frac{d\hat{v}}{dy} + \beta\hat{\eta}\right) = i\alpha c\sigma\hat{\Theta}, \tag{13}$$

where $F_m = F/K_0$ and

$$\hat{\eta} = \beta\hat{u} - \alpha\hat{w}. \tag{14}$$

For the velocity, the usual no-slip condition is taken. For the perturbed temperature, however, two types of boundary conditions are employed:

BC type I—zero temperature perturbation:

$$\hat{v} = \frac{d\hat{v}}{dy} = \hat{\eta} = \hat{\Theta} = 0, \quad y = \pm 1. \tag{15}$$

BC type II—zero heat flux perturbation:

$$\hat{v} = \frac{d\hat{v}}{dy} = \hat{\eta} = \frac{d\hat{\Theta}}{dy} = 0, \quad y = \pm 1. \tag{16}$$

C. Method of solution

In order to solve the coupled differential equations (11)–(13) along with any of the boundary conditions (15) or (16), the Galerkin technique has been used. For boundary condition type I, we have taken

$$\hat{v} = \sum_{n=0}^{N} a_n\xi_n(y), \quad \hat{\eta} = \sum_{n=0}^{N} b_n\zeta_n(y), \quad \hat{\Theta} = \sum_{n=0}^{N} d_n\zeta_n(y), \tag{17}$$

with the corresponding base functions

$$\xi_n(y) = (1-y^2)^2 P_n(y), \quad \zeta_n(y) = (1-y^2)P_n(y), \tag{18}$$

which satisfy (15). In Eq. (18), $P_n(y)$ denotes the Legendre polynomial of order n. Multiplying Eq. (11) by ξ_m, Eqs. (12) and (13) by ζ_m, and integrating them along y, one obtains

$$\sum_{n=0}^{N} a_n\int_{-1}^{1}[\xi_n''\xi_m'' + 2(\alpha^2+\beta^2)\xi_n'\xi_m' + (\alpha^2+\beta^2)\xi_m\xi_n]dy + \frac{i\alpha P_g}{\varepsilon^2}\sum_{n=0}^{N} a_n\int_{-1}^{1}\left[\left(\frac{d^2U_0}{dy^2} + (\alpha^2+\beta^2)U_0\right)\xi_n\xi_m - U_0\xi_n''\xi_m\right]dy$$

$$+ \frac{1}{Da^*}\sum_{n=0}^{N} a_n\int_{-1}^{1}\left[\frac{(K_2\beta^2+\alpha^2)}{(\alpha^2+\beta^2)}\xi_m'\xi_n' + K_1(\alpha^2+\beta^2)\xi_m\xi_n\right]dy - \frac{1}{Da^*}i\frac{\alpha\beta(K_2-1)}{(\alpha^2+\beta^2)}\sum_{n=0}^{N} b_n\int_{-1}^{1}\zeta_n'\xi_m\,dy$$

$$+ (\alpha^2+\beta^2)F_m\sum_{n=0}^{N} a_n\int_{-1}^{1}|U_0|\xi_m\xi_n\,dy - i\alpha\,Ra\sum_{n=0}^{N} d_n\int_{-1}^{1}\zeta_n'\xi_m\,dy + \left(\frac{\alpha^2}{(\alpha^2+\beta^2)}+1\right)F_m\sum_{n=0}^{N} a_n\int_{-1}^{1}|U_0|\xi_n'\xi_m'\,dy$$

$$- i\frac{\alpha\beta}{(\alpha^2+\beta^2)}F_m\sum_{n=0}^{N} b_n\int_{-1}^{1}|U_0|\xi_m'\zeta_n\,dy = i\alpha c\frac{P_g}{\varepsilon}\sum_{n=0}^{N} a_n\int_{-1}^{1}(\xi_n'\xi_m' + (\alpha^2+\beta^2)\xi_m\xi_n)dy, \tag{19}$$

$$- \frac{P_g}{\varepsilon^2}\beta\sum_{n=0}^{N} a_n\int_{-1}^{1}U_0(\zeta_m'\xi_n + \zeta_m\xi_n')dy - \beta\,Ra\sum_{n=0}^{N} d_n\int_{-1}^{1}\zeta_m\zeta_n\,dy + \sum_{n=0}^{N} b_n\int_{-1}^{1}[(\alpha^2+\beta^2)\zeta_m\zeta_n + \zeta_m'\zeta_n']dy$$

$$+ i\frac{\alpha P_g}{\varepsilon^2}\sum_{n=0}^{N} b_n\int_{-1}^{1}U_0\zeta_m\zeta_n\,dy + \frac{1}{Da^*}\left(\sum_{n=0}^{N} b_n\frac{(K_2\alpha^2+\beta^2)}{(\alpha^2+\beta^2)}\int_{-1}^{1}\zeta_m\zeta_n\,dy + i\frac{(1-K_2)\alpha\beta}{(\alpha^2+\beta^2)}\sum_{n=0}^{N} a_n\int_{-1}^{1}\xi_n'\zeta_m\,dy\right)$$

$$+ i\frac{\alpha\beta}{(\alpha^2+\beta^2)}F_m\sum_{n=0}^{N} a_n\int_{-1}^{1}|U_0|\zeta_m\xi_n'\,dy + \left(\frac{\beta^2}{(\alpha^2+\beta^2)}+1\right)F_m\sum_{n=0}^{N} b_n\int_{-1}^{1}|U_0|\zeta_m\zeta_n\,dy = ic\alpha\frac{P_g}{\varepsilon}\sum_{n=0}^{N} b_n\zeta_m\zeta_n\,dy, \tag{20}$$

Phys. Fluids, Vol. 14, No. 5, May 2002

Stability of mixed convection in anisotropic porous channel   1621

$$-\sum_{n=0}^{N} a_n \int_{-1}^{1} \Theta_0(\zeta'_m\xi_n+\zeta_m\xi'_n)dy + i\frac{\alpha}{P_g\,\mathrm{Pr}^*(\alpha^2+\beta^2)}\sum_{n=0}^{N} a_n \int_{-1}^{1}\zeta_m\xi'_n\,dy + i\alpha\sum_{n=0}^{N} d_n \int_{-1}^{1}\mathrm{U}_0\zeta_m\zeta_n\,dy$$

$$+\frac{1}{P_g\mathrm{Pr}^*}\sum_{n=0}^{N} d_n \int_{-1}^{1}[\mathrm{k}_1\zeta'_m\zeta'_n+(\alpha^2+\mathrm{k}_2\beta^2)\zeta_m\zeta_n]dy + \frac{\beta}{P_g\,\mathrm{Pr}^*(\alpha^2+\beta^2)}\sum_{n=0}^{N} b_n \int_{-1}^{1}\zeta_m\zeta_n\,dy = i\alpha c\sigma\sum_{n=0}^{N} d_n \int_{-1}^{1}\zeta_m\zeta_n\,dy,$$

$$(21)$$

in which the primed quantities denote differentiation with respect to y. Note that for boundary condition type II, the base function for $\hat{\Theta}$ of Eq. (13) has to be replaced by ϕ_n, which is defined by

$$\phi_n(y) = \begin{cases} (1-y^2)P_n(y)+2P_1 & \text{for odd } n, \\ (1-y^2)P_n(y)+\frac{2}{3}P_2 & \text{for even } n. \end{cases} \tag{22}$$

Finally, Eqs. (19–21) can be written as the general eigenvalue problem

$$A\mathbf{x}=cB\mathbf{x}, \tag{23}$$

with c being the eigenvalue and $\mathbf{x}$ denotes the eigenvector of field entities. A and B are the matrix representations of the set of linear volume equations and boundary conditions. The above-presented system can be solved by standard routine. Here, the DGVLCG of the IMSL library[39] was employed. The routine is based on the QZ algorithm due to Moler and Stewart.[40] The first step of this algorithm is to simultaneously reduce A to upper Heisenberg form and B to upper triangular form. Then, orthogonal transformations are used to reduce A to quasi-upper-triangular form while keeping B upper triangular. The generalized eigenvalues and eigenvectors for the reduced problem are then computed.

D. Energy analysis

Once the critical value of Ra is known, the physical reason for the instability can be explained by considering the energy transfer between the basic state and the neutral mode. The rate of change of nondimensional kinetic and thermal energy are

$$\frac{P_g}{\varepsilon}\frac{\partial}{\partial t}\left\langle\frac{1}{2}(u'^2+v'^2+w'^2)\right\rangle$$

$$=-\frac{P_g}{\varepsilon^2}\left\langle u'v'\frac{d\mathrm{U}_0}{dy}\right\rangle+\mathrm{Ra}\langle u'\Theta'\rangle-\frac{1}{\mathrm{Da}^*}\langle u'^2+\mathrm{K}_1v'^2$$

$$+\mathrm{K}_2w'^2\rangle-F_m\langle|\mathrm{U}_0|(2u'^2+v'^2+w'^2)\rangle-\langle(\nabla u')^2$$

$$+(\nabla v')^2+(\nabla w')^2\rangle=\mathrm{E_s}+\mathrm{E_b}+\mathrm{E_D}+\mathrm{E_F}+\mathrm{E_d}, \tag{24}$$

$$\sigma\frac{\partial}{\partial t}\left\langle\frac{1}{2}\Theta'^2\right\rangle$$

$$=-\frac{1}{P_g\,\mathrm{Pr}^*}\left\langle\left(\frac{\partial\Theta'}{\partial x}\right)^2+\mathrm{k}_1\left(\frac{\partial\Theta'}{\partial y}\right)^2+\mathrm{k}_2\left(\frac{\partial\Theta'}{\partial z}\right)^2\right\rangle$$

$$-\left\langle\Theta'v'\frac{d\Theta_0}{dy}\right\rangle-\frac{1}{P_g\,\mathrm{Pr}^*}\langle\Theta'u'\rangle=T_d+T_c+T_b, \tag{25}$$

where the angular brackets $\langle\rangle$ represent the volumetric average over the volume of disturbance wave. The disturbance kinetic energy terms, $\mathrm{E_s}$, $\mathrm{E_b}$, $\mathrm{E_D}$, $\mathrm{E_F}$, and $\mathrm{E_d}$ in (24) are due to work done by shear force, thermal buoyancy, surface drag (Darcy term), form drag (Forchheimer term), and viscous force, respectively. In Eq. (25), quantities termed T_c, T_d, and T_b are associated with disturbance thermal energy due to convection, rate of heat diffusion, and disturbance thermal energy due to work done by the thermal buoyancy. All derivatives are approximated by fourth-order finite difference in the given domain except at boundaries. Integrals are calculated using fourth-order Simpson's extended rule. The relative error in the kinetic energy balance, δ_K, is defined as the residual normalized by the sum of the absolute values of shear production of disturbance kinetic energy and disturbance kinetic energy due to thermal buoyant potential, and are given by

$$\delta_K=\frac{|\mathrm{E_s}+\mathrm{E_b}+\mathrm{E_D}+\mathrm{E_F}+\mathrm{E_d}|}{|\mathrm{E_s}|+|\mathrm{E_b}|},$$

while

$$\delta_T=\frac{|T_c+T_d+T_b|}{\max\{|T_c|,|T_d|,|T_b|\}}$$

is used to account for the error of the thermal energy balance.

III. RESULTS

A rigorous stability analysis has been performed here to answer the question of the condition for the occurrence of the maximum stability. As can be seen from Table I, when the wave number in the spanwise direction, β, is equal to zero, the minimum critical Ra is achieved. This implies that the least stable mode is two-dimensional. Hence, throughout the analysis presented here, $\beta=0$ has been considered. This result coincides also with those found for the stability consideration in both viscous (Chen and Chung[11]) as well as porous media (Tyvand and Storesletten[24]). Furthermore, the Prandtl number Pr*, Forchheimer number F, porosity ϵ, and heat capacity ratio σ, always take the values 1, 1, 0.9, and 1, respectively. In the following, the Reynolds number Re $=P_g\bar{\mathrm{U}}_0$ has been employed to find the neutral stable mode for other different parameters studied here. Throughout this section, critical Ra_c and α_c have been represented by Ra and α, respectively. A logarithmic scale has been used along the vertical axis to display all the instability boundaries on a single (Re,Ra) plane. In all contour plots, dashed lines denote negative values whereas solid lines stand for positive

1622   Phys. Fluids, Vol. 14, No. 5, May 2002

P. Bera and A. Khalili

TABLE I. Dependence of the critical Rayleigh number on β for different cases (Re=500).

K_1	k_1	Da*	F	β	Ra
0.1	1	10^{-2}	1	0	*100.16*
0.1	1	10^{-2}	1	0.5	100.75
0.1	1	10^{-2}	1	1.0	102.25
0.1	1	10^{-2}	1	1.5	105.75
1	1	10^{-2}	1	0	*160.94*
1	1	10^{-2}	1	0.5	164.50
1	1	10^{-2}	1	1	177.50
1	1	10^{-2}	1	1.5	223.00
10	1	10^{-2}	1	0	*1 368.75*
10	1	10^{-2}	1	0.5	1 715.00
10	1	10^{-2}	1	1	3 270.00
10	1	10^{-2}	1	1.5	4 437.50
0.1	0.2	10^{-2}	1	0	*18.16*
0.1	0.2	10^{-2}	1	0.5	18.22
0.1	0.2	10^{-2}	1	1	18.34
0.1	0.2	10^{-2}	1	1.5	18.59
0.1	5	10^{-2}	1	0	*647.50*
0.1	5	10^{-2}	1	0.5	657.50
0.1	5	10^{-2}	1	1	687.50
0.1	5	10^{-2}	1	1.5	757.50
0.1	1	10^{-1}	1	0	*42.89*
0.1	1	10^{-1}	1	0.5	43.02
0.1	1	10^{-1}	1	1	43.45
0.1	1	10^{-1}	1	1.5	44.23
0.1	1	10^{-3}	1	0	*2 725.00*
0.1	1	10^{-3}	1	0.5	2 925.00
0.1	1	10^{-3}	1	1	4 175.00
0.1	1	10^{-3}	1	1.5	10 175.00
0.1	1	10^{-2}	10^4	0	*143.44*
0.1	1	10^{-2}	10^4	0.5	144.50
0.1	1	10^{-2}	10^4	1	146.50
0.1	1	10^{-2}	10^4	1.5	151.50

TABLE II. Dependence of the critical Rayleigh number on number of grid points as well as on order of the base polynomials ($K_1=0.1$, $k_1=1$, Da* $=10^{-2}$, F=1).

Grid dimension	N	Re	Ra	α
51	25	400	102.19	2.62
51	30	400	102.19	2.62
101	25	400	107.19	2.58
101	30	400	107.19	2.60
101	35	400	107.81	2.60
201	25	400	108.43	2.54
201	30	400	108.43	2.54
201	35	400	108.43	2.50
301	25	400	108.43	2.56
301	30	400	108.43	2.60
301	35	400	108.43	2.60
401	25	400	108.43	2.60
401	30	400	108.43	2.60
401	35	400	108.43	2.60

A. Validation of code

In order to validate the results presented in this work, the following steps were carried out. First, the response of instability boundaries to grid size (M) and order of base polynomial (N) variation were tested. Second, we examined whether or not the change of total disturbance kinetic and thermal energy vanishes at the instability boundaries. Third, the general results presented here were compared with those given in the literature for special cases.

Using the base solutions, the critical values for the Rayleigh number and streamwise wave number were obtained for different number of grid points as well as order of base polynomials, and are shown in Table II. As can be seen from Table II, a further increase of M and N beyond 301 and 30, respectively, does not have an impact on Ra and α. Hence, in the linear stability analysis given below 301 grid points and an order of polynomial 30 have been considered as standard values. A severe test (see Table III) for both basic state and linear stability calculation is provided by the energy balance. For all calculations presented in the following, the errors in thermal energy balance, δ_T, and in kinetic energy balance, δ_K, are $\leqslant 0.3\%$. Note that for solving basic state flow iteratively, a residual limit of 10^{-11} was set for best convergence, though it was noticed that 10^{-9} would have been sufficient. Due to these relatively low errors, one may conclude that all flow and stability features are well resolved. A final check is made by a comparison between the published results for a

values. In addition, for streamfunction, solid and dashed lines are associated with a clockwise and counter-clockwise rotation, respectively.

Depending on the nature of boundary walls and fluid, two different boundary conditions for perturbed temperature are possible. If the bounding walls of the fluid layer have high heat conductivity and large heat capacity, then its temperature would be spatially uniform and unchanging in time. In other words, the temperature of the boundary would be unperturbed by any flow or temperature perturbation in the fluid domain. Therefore, it would be appropriate to take the disturbed wall temperature equal to zero, which is referred to as the boundary condition of the first kind (BC I). However, this fixed temperature boundary conditions at the surface of the fluid layer may be too restrictive because there will be heat exchange between the solid conductive wall and the fluid. Hence, a constant heat flux at the wall would be the other possibility (BC II). In order to cover a wider range of applications, both types of boundary conditions have been taken into account here. For each of these cases, the effect of different parameters has been studied in detail. Before discussing the effect of different parameters on the stability of the system, a verification of the code is given.

TABLE III. Kinetic and thermal energy errors for different permeability ratios (Re=500, $K_1=0.1$, $k_1=1$, F=1, Da*$=10^{-2}$).

K_1	$\delta_K(\%)$	$\delta_T(\%)$	Ra	α
0.1	0.15	0.23	100.16	2.54
1	0.22	0.28	160.94	2.02
10	0.07	0.30	1368.75	1.04

TABLE IV. Comparison between published results (Ref. 11) and present results ($\epsilon = 1$, $Pr^* = 0.7$, $K_1 = 1$, $k_1 = 1$, $Da^* = 10^5$, $F = 0$).

Re	Ra (present)	Ra (Chen—Ref. 11)	α (present)	α (Chen—Ref. 11)
100	43.57	41.65	0.85	0.87
215	37.50	37.60	1.05	0.98
500	32.62	32.65	1.21	1.22
1000	30.24	30.26	1.31	1.35

fluid-filled vertical channel as a particular case of our results. Table IV compares the critical Ra and α of the present study with those of Chen and Chung[11] for $\epsilon = 1$, $F = 0$, $Da^* = 10^5$, $Pr^* = 0.7$. As can be seen, the agreement is good. These various tests provide a strong validation of our numerical results.

B. Zero temperature perturbation

The effect of different parameters on the stability of flow and heat transfer, i.e., on the critical Raleigh number Ra and critical wave number α as a function of Reynolds number Re, has been studied. The parameters considered are permeability ratio K_1, thermal diffusivity ratio k_1, and modified Darcy number Da^*.

1. Dependence of Ra and α on permeability

In this section, $k_1 = 1$ and $F = 1$ have been set for all cases except when, for the sake of comparison, the fluid-only case is considered, for which $\epsilon = 1$, $F = 0$, and $Da^* = 10^5$ have been taken.

Our numerical experiments showed that the disturbance velocity component along the z axis, $\hat{w}$, was always almost zero. At the same time, $\beta = 0$ was found to provide the maximum instability. Putting these facts together, from (14) one obtains $\hat{\eta}$ equal to zero. Further, inserting $\hat{\eta} = 0$ in (11) and (13) implies that K_2 does not come into the picture. Hence, the effect of permeability variations can be studied through K_1. Note that for a given Da^* (which fixes K_x), variation of K_1 is due to an independent change of K_y. Therefore, to study the effect of permeability along the main flow direction (x), Darcy number has to be taken into account.

Figure 3(a) shows the instability boundaries on (Re,Ra)

plane for a viscous fluid, for an isotropic porous medium ($K_1 = 1$), anisotropic medium with high permeability ($K_1 = 0.1$), and anisotropic porous medium with low permeability ($K_1 = 10$) along the y axis. As can be observed from Fig. 3, fully developed flow is more stable in the case of porous medium compared to that of a viscous fluid, and low permeable medium is more stable than high permeable one. This result can be explained by examining the extreme values of disturbance stream function (ψ) and temperature (Θ') for a given Re, e.g., Re = 1000 (Table V). As demonstrated in Table V, among all cases considered, a low permeable medium ($K_1 = 10$) leads to the minimum disturbance in both ψ ($= 0.08$) and Θ' ($= 0.16$), whereas viscous fluid gives the maximum disturbance ($\psi = 0.11$, $\Theta' = 0.51$). Consequently, the system has the maximum stability in the former and minimum stability in the latter case.

An important feature of the instability boundaries on the (Re,Ra) plane is that, for all cases, a drastic change of the Ra is observed before a threshold value of Reynolds number [Fig. 3(a)], whereas beyond this value, a smooth and slow change occurs. A similar behavior in the vicinity of the threshold value of Re may also be observed in the wave number [Fig. 3(b)]. At a quantitative level, this phenomena can be explained by the distinct behavior of the disturbance kinetic energy components undergoing points of extremum around the threshold values of Re [Figs. 4(a)–4(d)], denoting that the energy supply to the flow instability attains a sudden change in these regions. The reason for this change can be seen in the fact that when the walls of the vertical channel are maintained at a uniform temperature, the upward forced flow is unconditionally stable for infinitesimal disturbance even for very large Reynolds numbers. However, in the case of nonisothermally heated vertical walls, the stability of the flow will also depend on the heating condition. Under the heating condition, a slow flow can carry denser fluid upward into the region of lighter fluid, as pointed out by Yao and Rogers.[9] While doing so, in addition to the energy due to shear force existing in a viscous fluid, for a porous medium, a new source of disturbance energy, namely the one caused by surface drag (associated with the modified Darcy term) appears in the region of high velocity. As a consequence, a point of inflection develops leading to a local high-shear
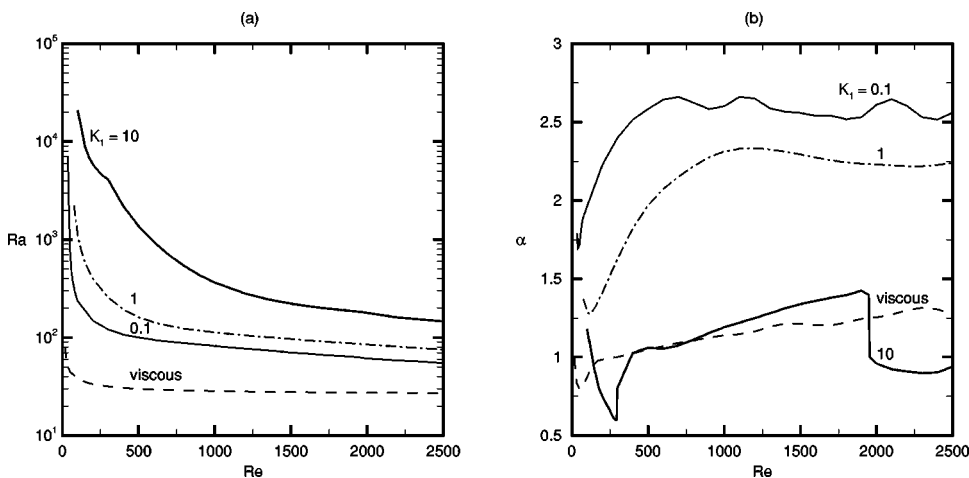

FIG. 3. Dependence of the critical Rayleigh number (a) and wave number (b) on Re for different permeability ratios.
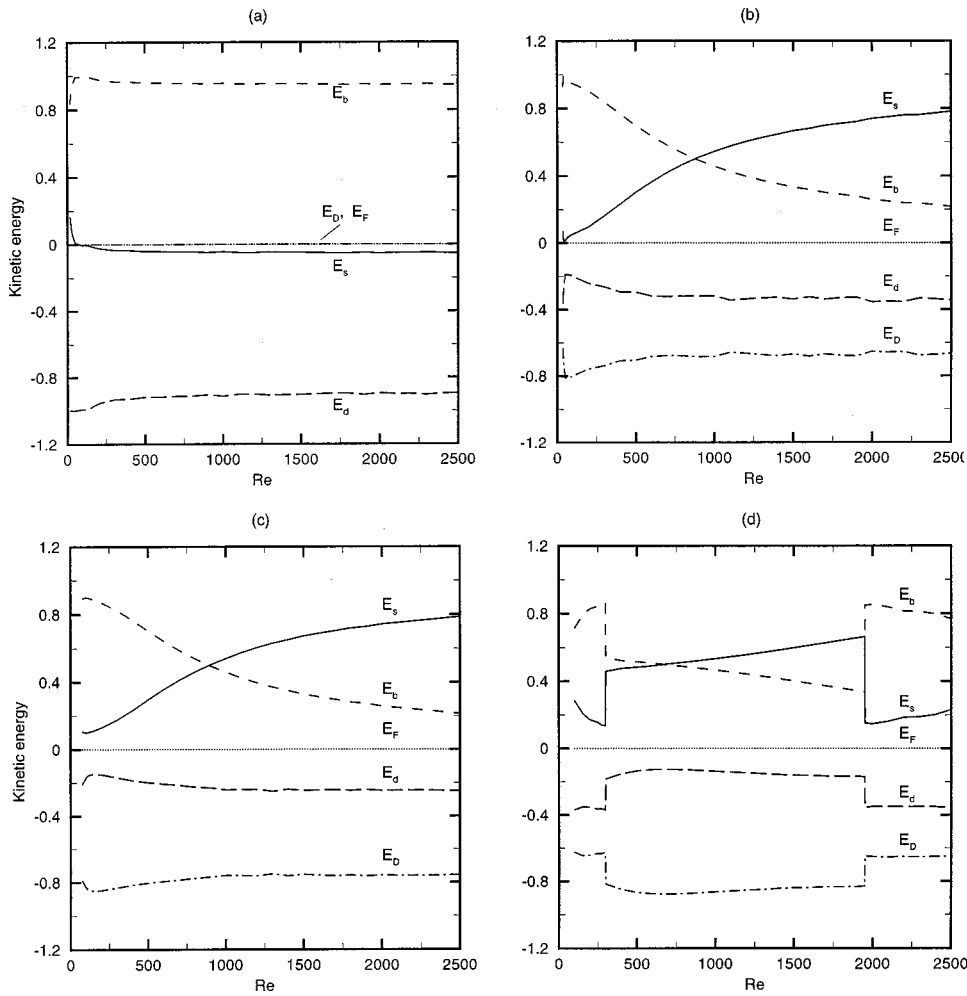
FIG. 4. The rate of change of kinetic energy as a function of Re (a) for viscous fluid, (b) $K_1 = 0.1$, (c) $K_1 = 1$, and (d) $K_1 = 10$.

layer. In this situation, small enhancement of Re makes the convection in the direction of main flow stronger, and more dense fluid can be transported upwards to destabilize the flow, and hence the critical heating condition falls drastically. As Re is increased further, the difference between fluid velocity in the denser and lighter zones reduces, which results in the reduction of the rate of change of critical Ra as a function of Re. The extreme jump in the behavior of kinetic energy for a low permeable medium [Fig. 4(d)] made us examine the flow pattern near the location where the threshold value of Re appears. The interesting finding was that the flow pattern undergoes a shift from bicellular to a unicellular one (see Fig. 5), and in the case of $K_1 \geqslant 6$, the latter pattern again shifts to a bicellular one. The pattern reshifting depends on the value of K_1. For example, for $K_1 = 10$, it appeared when Re is approximately 1951. However, no bicel-

lular patterns occurred in the disturbance stream function when the channel was filled with a viscous or isotropic porous medium (figures not shown).

Studying the variation of the kinetic energy helps to find out which types of instabilities occur as the Reynolds number changes. For the case of a viscous fluid [Fig. 4(a)], the kinetic energy generated by buoyancy force (E_b) is the dominant term in balancing the dissipation of kinetic energy due to viscosity (E_d) throughout the Re range, and except for a weak forced flow, it leads to the existence of a pure thermal instability. This phenomena has been observed in the literature.[11]

However, in the presence of a porous medium the instability mode differs. For isotropic or anisotropic porous media, namely, thermal, mixed and shear instability may occur as Reynolds number increases. Figures 4(b) and 4(c) show that the sum of the dissipation of kinetic energy due to surface drag (E_D) and due to viscosity (E_d) is balanced by kinetic energy due to thermal buoyancy (E_b) for extremely low Re, kinetic energy due to shear E_s for high Re, which in turn, gives thermal instability at low Re and shear instability at high Re. For moderate values of Re the energy dissipation is balanced by both E_s and E_b, and mixed mode instability is given. In short, it can be stated that for low permeable media ($K_1 \geqslant 6$), the transition of one instability mode to an-

TABLE V. Maximum and minimum magnitude of disturbance stream function and temperature for different permeable media ($k_1 = 1$, $Da^* = 10^{-2}$, $F = 1$) and viscous fluid ($k_1 = 1$, $Da^* = 10^5$, $F = 0$) at $Re = 1000$.

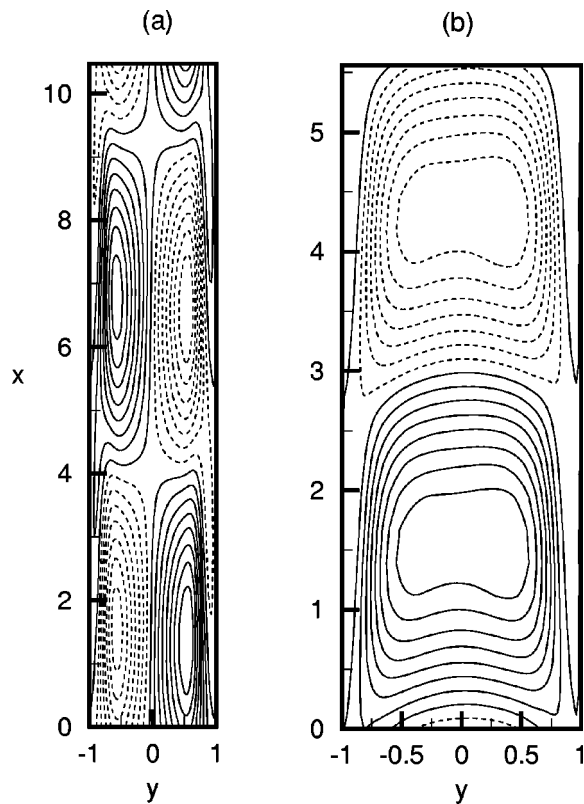| K_1	10	1	0.1	Viscous
ψ^{max}_{min}	± 0.08	± 0.084	± 0.11	± 0.11
Θ'^{max}_{min}	± 0.16	± 0.29	± 0.28	± 0.51

FIG. 5. The disturbance streamlines for $K_1=10$; (a) Re=299 (ψ_{min} $=-0.052$, $\psi_{max}=0.052$) and (b) Re=300 ($\psi_{min}=-0.044$, $\psi_{max}=0.044$) for one period.

other is abrupt (in the case of $K_1=10$ at Re=300 and 1951), whereas for isotropic [Fig. 4(c)] as well as high permeable anisotropic media [Fig. 4(b)], the change takes place in a smooth manner.

The analysis of thermal energy balance has been performed for the above-mentioned parameter range. However, because of the qualitative similarity among the behavior of all cases, the diffusion of thermal energy (T_d) was balanced by disturbance thermal energy due to convection (T_c) in almost the entire Re range, except for small Re below the threshold value where the disturbance thermal energy due to buoyancy (T_b) has a sizable contribution.

The neutral stability curves on the (Re,Ra) and (Re,α) plane for $K_1=0.1$, $k_1=1$, and different Darcy numbers are shown in Fig. 6. As can be seen from Fig. 6(a), first, with a decrease in Da*, more stable flow is observed, which is based on the fact that enhancing Da* is due to an increase of permeability in the vertical direction. As a consequence, the flow strength increases and becomes unstable even for lower heating. Second, when Da* moves from 10^{-1} to 10^{-2}, the logarithmic value of Ra increases by the factor ≈ 1.2 throughout the Re range above the threshold value. However, for decreasing Da* from 10^{-2} to 10^{-3}, this factor increases and lies between 1.9 and 1.6 with growing Re. Simultaneously, the frequency of the disturbance in the main flow direction exceeds more than 3.6 for Re>1600 and Da* $=10^{-1}$ [Fig. 6(b)] or its wavelength of disturbance reduces to below 87.3% of channel width. This indicates that the local disruption of the velocity field which is induced by temperature fluctuation causes the flow instability in the channel. With the help of the disturbance energy, streamline, and temperature contours, more insight into the physics involved can be given. A comparison of Figs. 7(a) and 7(b) shows that the dissipation of kinetic energy due to surface drag increases as Da* decreases from 10^{-1} to 10^{-3}, whereas the same due to viscosity decreases (in magnitude). Figures 7(a) and 7(b) also reveal that for anisotropic porous media with Da*$=10^{-3}$, the contributions of E_s in the production of kinetic energy, and E_F and E_d in the dissipation of kinetic energy are negligible. Note that for a small Darcy number (Da*$=10^{-3}$), only thermal instability occurs, whereas for relatively large Da*, thermal, mixed, and shear instabilities exist simultaneously. Furthermore, comparing the flow and temperature field for Da*$=10^{-1}$ with that of Da*$=10^{-3}$, the following observations can be made. As Darcy number decreases, the shape of the streamlines changes from oblate triangles to quasi-squares [Figs. 8(a) and 8(b)], which have their vertical sides parallel to the channel wall. This pattern denotes the existence of a vertically dominant motion with near zero horizontal component, which reduces the heat transfer by convection in the y direction. From the other side, the temperature isolines move from the center toward the channel walls [Figs. 9(a) and 9(b)], and become parallel to them in the near-wall region. These facts together denote that
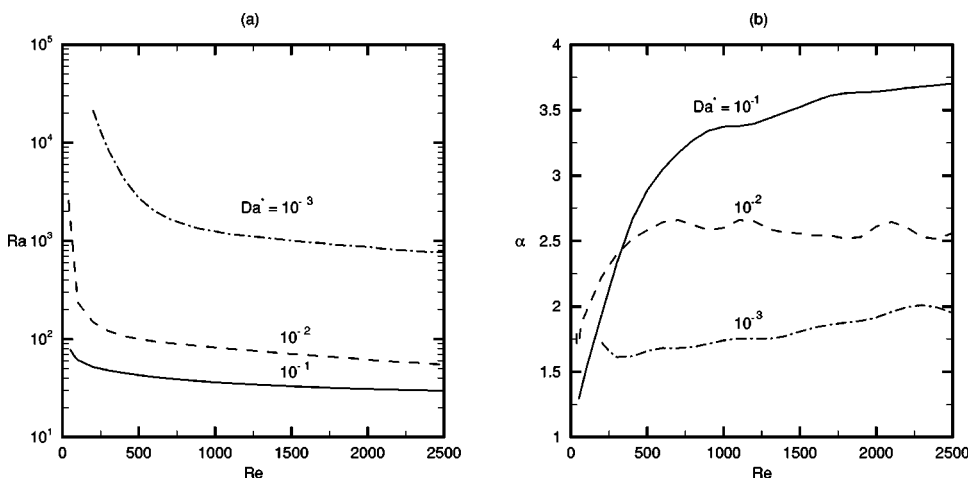

FIG. 6. Dependence of the critical Rayleigh number (a) and wave number (b) on Re for different modified Darcy number.
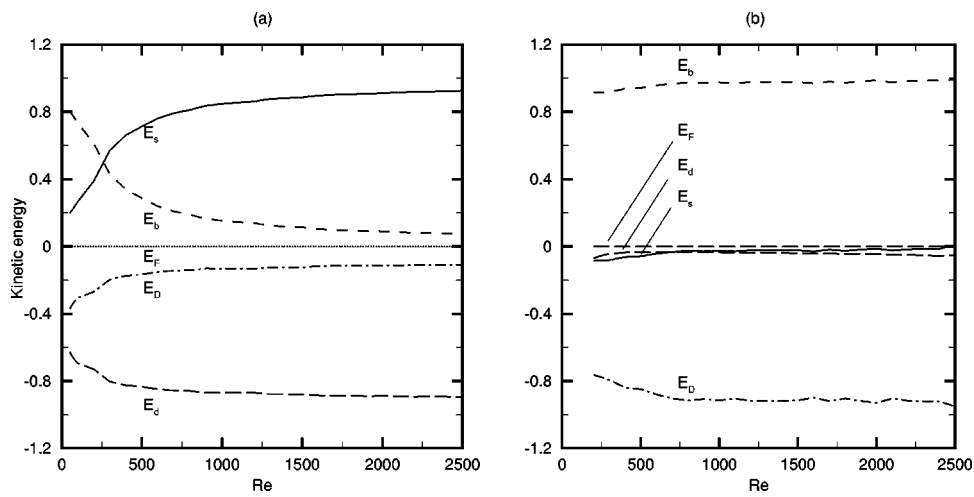
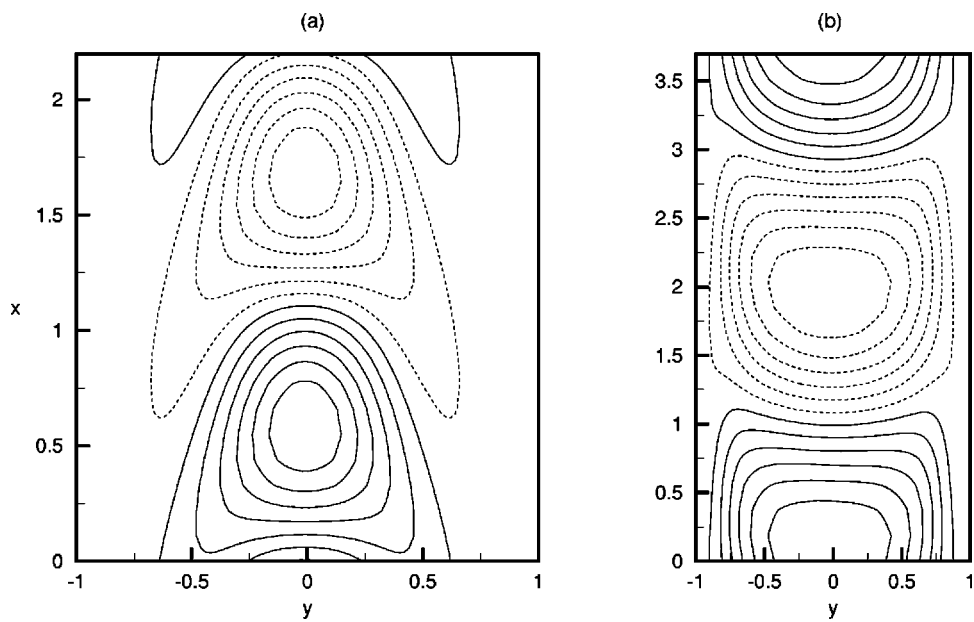FIG. 7. The rate of change of kinetic energy as a function of Re; (a) Da* $=10^{-1}$, (b) Da* $=10^{-3}$.

FIG. 8. The disturbance streamlines for Re$=500$ and $K_1=0.1$; (a) Da* $=10^{-1}$ ($\psi_{min}=-0.182$, $\psi_{max}=0.182$) and (b) Da* $=10^{-3}$ ($\psi_{min}=-0.053$, $\psi_{max}=0.053$) for one period.
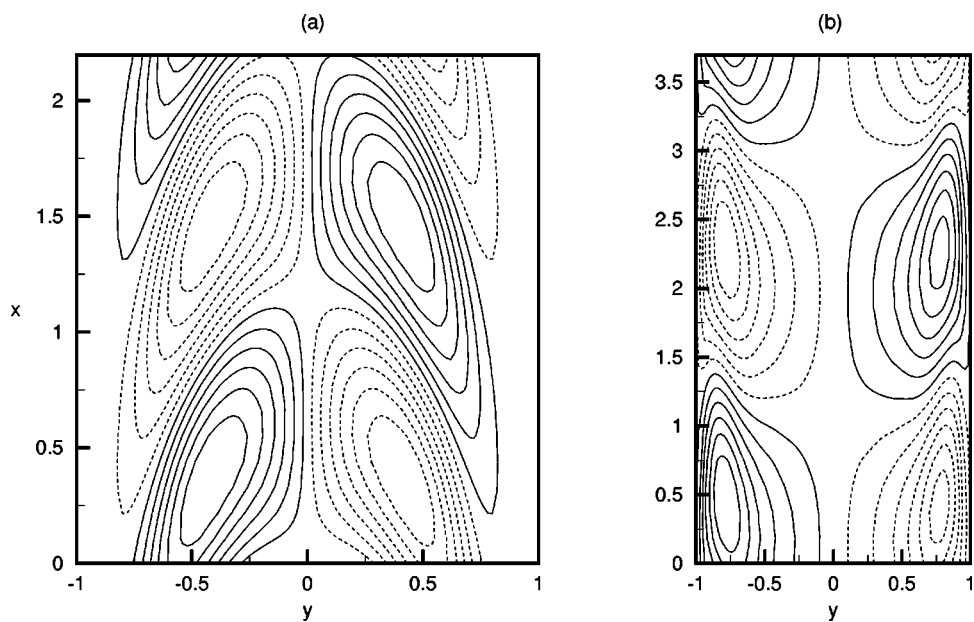

FIG. 9. The disturbance temperature field for Re$=500$ and $K_1=0.1$; (a) Da* $=10^{-1}$ ($\Theta_{min}=-0.235$, $\Theta_{max}=0.235$), (b) Da* $=10^{-3}$ ($\Theta_{min}=-0.06$, $\Theta_{max}=0.06$) for one period.
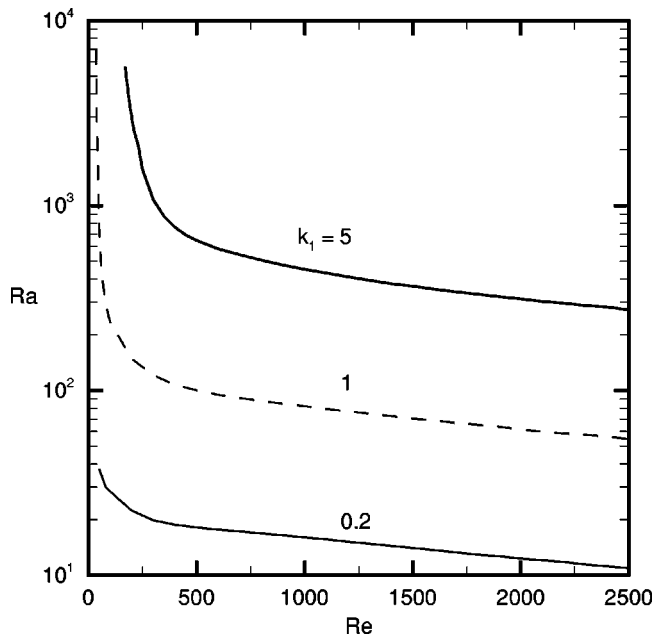
FIG. 10. Dependence of the critical Rayleigh number on Re for different thermal diffusivity ratios.

the transfer of the disturbance temperature takes place mainly by diffusion, leading to a more stable flow configuration. This can be also confirmed when the largest disturbance stream function and temperature are compared. Both these values fall drastically from 0.183 to 0.053 and from 0.235 to 0.06, respectively, when the Darcy number decreases from 10^{-1} to 10^{-3}.

2. Dependence of Ra and α on thermal diffusivity

The instability boundaries on the (Re,Ra) plane for k_1 = 0.2, 1, and 5 when K_1 = 0.1, F = 1, Da* = 10^{-2} are shown in Fig. 10. As thermal diffusivity increases, the critical Rayleigh number increases, making the system more stable. To describe the shift of the neutral stability curve as a function of thermal diffusivity ratio, the disturbance stream functions and temperature were plotted for a specific Re (=500) for k_1 = 0.2 and 5 (see Figs. 11 and 12). By more closely examining the maximum values of ψ and Θ', it is found that ψ increases from 0.023 to 0.12, and that of Θ' decreases from 0.39 to 0.041. Obviously, the first trend is contradicting the above-noted observation on the system stability, whereas the
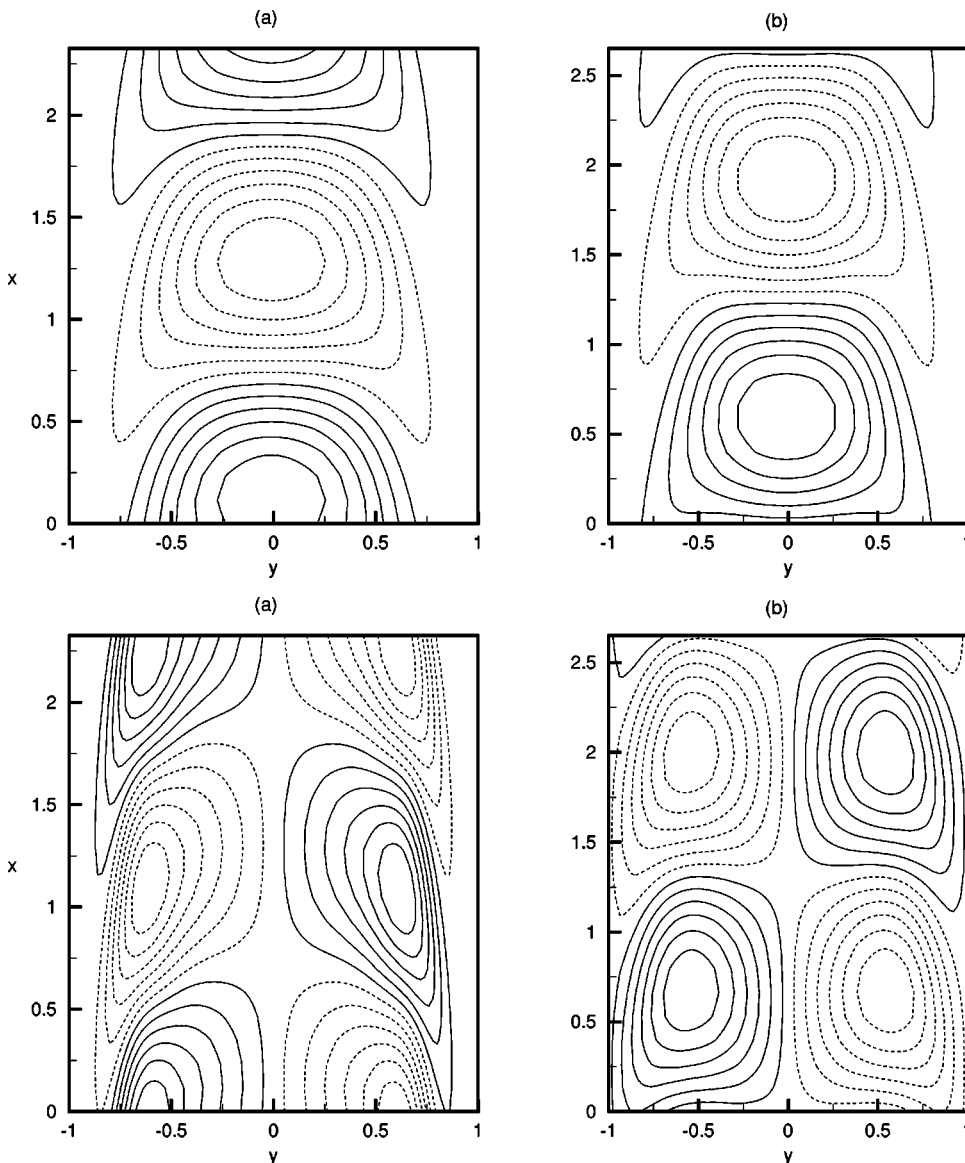

FIG. 11. The disturbance streamlines for Re=500 and K_1=0.1; (a) k_1=0.2 (ψ_{min}=-0.023, ψ_{max}=0.023), (b) k_1=5 (ψ_{min}=-0.12, ψ_{max}=0.12) for one period.

FIG. 12. The disturbance temperature field for Re=500 and K_1=0.1; (a) k_1=0.2 (Θ_{min}=-0.39, Θ_{max}=0.39), (b) k_1=5 (Θ_{min}=-0.041, Θ_{max}=0.041) for one period.
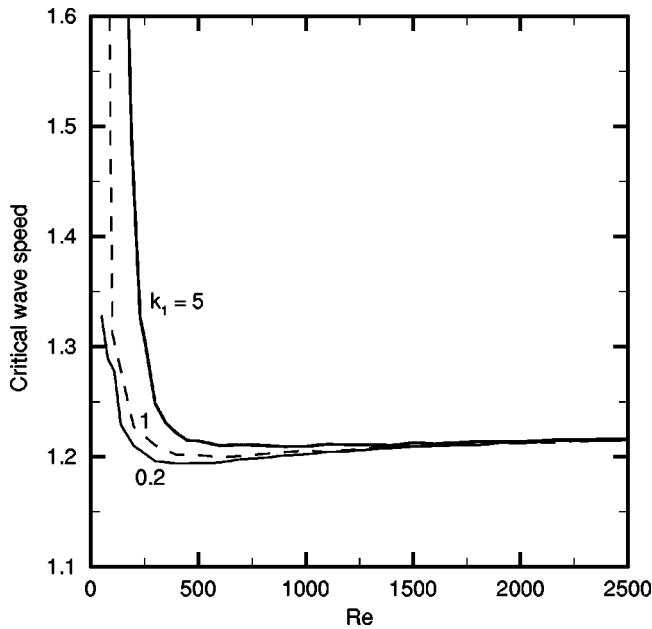
FIG. 13. Dependence of the critical wave speed on Re for different thermal diffusivity ratios.

second one is in favor of it. Here, the question of which of the above-mentioned trends has more influence still remains to be determined. To explain this behavior, use is made of the energy spectra. The disturbance kinetic energy was analyzed for low, moderate, and high values of thermal diffusivity ratios. It was found that the stability mode is generally a mixed mode instability [as the results were similar to those presented in Fig. 4(b), they are not displayed here]. In addition, for Re=500, the contribution of energy production due to the buoyancy term was found to be almost twice that of the shear term. Quantitatively, E_b and E_s changed from 0.665 to 0.675, and 0.335 to 0.325, respectively, as k_1 changed from 0.2 to 5. This change can be regarded as a clear indication that the disturbance temperature is the key factor in deciding the location of the neutral stability curve in the Re–Ra plane. Furthermore, since the Prandtl number is kept constant (k_x is fixed), for high thermal diffusivity ratios, the conduction effect in the streamwise direction is empha-

sized, and in consequence, any thermal fluctuation in the flow field will damp out quickly. When the thermal diffusivity ratio is very small, in contrast, thermal fluctuations cannot be smoothed out by conduction and remain localized.

A further interesting feature, namely, the response of the wave speed ($c_r = \hat{c}_r/\bar{U}_0$) to thermal diffusivity variations, is shown in Fig. 13. For all cases of k_1, it was observed that c_r falls rapidly before a threshold value of Re is reached. After this value, changes are slow and monotonic, and the values are larger than unity. Recalling that the wave speed was non-dimensionalized by the average base velocity, it is interesting to note that for the anisotropic media studied, the minimum wave speed is always greater than average value of the base velocity. A similar finding has been presented by Chen and Chung[11] for a channel filled with a fluid having a Prandtl number of 7.

C. Zero heat flux perturbation

Similar to boundary condition I, a brief study of the effect of different anisotropic parameters on instability boundaries in (Re,Ra) and (Re,α) planes has been undertaken for boundary condition II. A variation of critical Rayleigh number as a function of Re for the perturbed BC type I and BC type II is displayed in Fig. 14(a) for two different values of K_1. As can be depicted from the figure, the Ra curve for zero heat flux coincides almost perfectly with that of zero temperature when $K_1 = 0.1$. A similar situation is given for $K_1 = 10$ beyond Re$\approx$1000, whereas significant deviations exist below it. This scenario holds also for the critical wave number [see Fig. 14(b)]. Hence, for low permeable media, zero temperature perturbation leads to a more stable flow than zero heat flux when Re lies below 1000. This statement is based on the analysis of the disturbance stream function as well as temperature, which showed that for BC II these variables exceed the same for BC I, denoting that BC type II is less stable compared to BC type I. The influence of the anisotropic thermal diffusivity ratio on the system stability is plotted in Figs. 15(a) and 15(b), which is qualitatively similar to that of anisotropic permeability ratio given previously. Quantitatively, however, there exist two different sub-intervals below Re=900, in which the dominance of stability
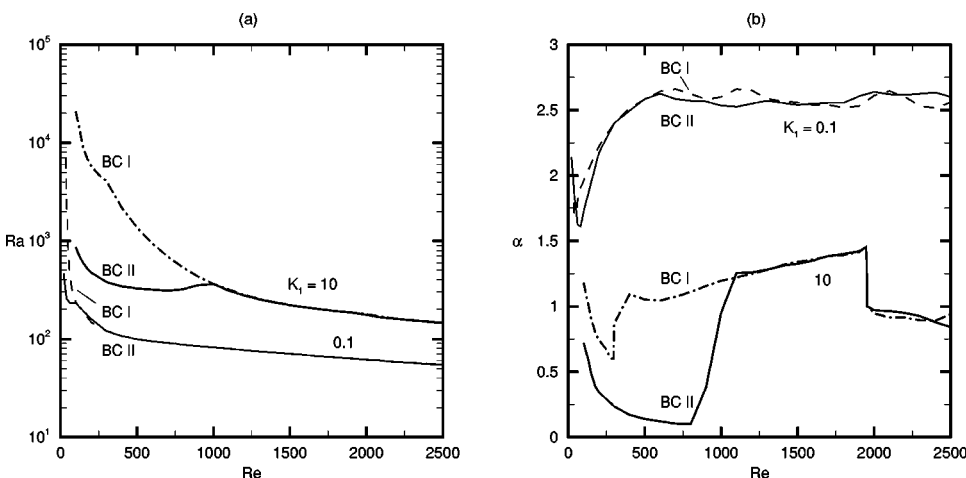

FIG. 14. Dependence of critical Rayleigh number (a) and wave number (b) for different permeability ratios ($k_1 = 1$, Da* $= 10^{-2}$) under zero heat flux boundary condition. Dashed and dash-dotted lines show zero temperature boundary condition.
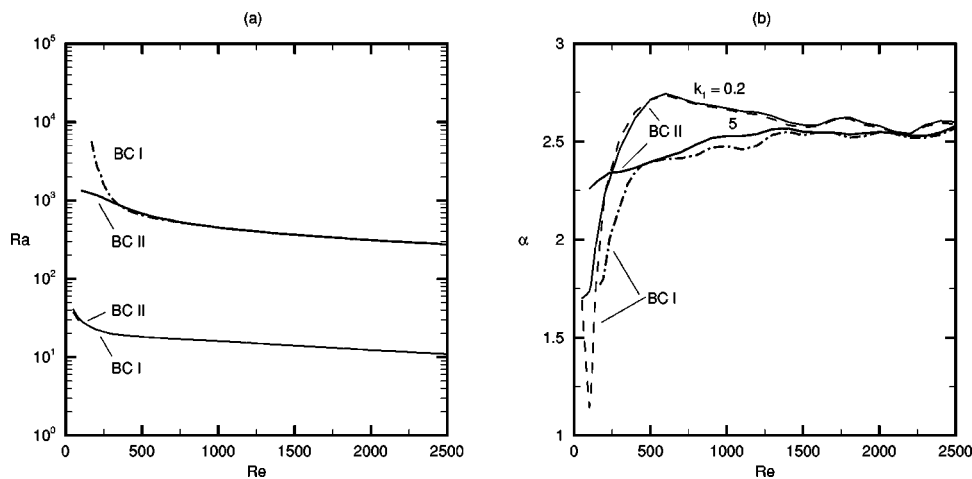
FIG. 15. Dependence of the critical Rayleigh number (a) and wave number (b) for different thermal diffusivity ratios ($K_1 = 1$, $Da^* = 10^{-2}$) under zero heat flux boundary condition. Dashed and dash-dotted lines show zero temperature boundary condition.

of zero temperature perturbation over zero heat flux fluctuates. We note that when the porous medium has a low permeability ($K_1 = 10$) or provides low diffusivity ($\alpha_1 = 0.2$), the threshold value for zero heat flux is larger than that for zero temperature boundary condition. This situation reverses, however, when the medium has higher permeability ($K_1 = 0.1$) or higher diffusivity ($\alpha_1 = 5$).

IV. CONCLUSIONS

In this work, we report the instability mechanism of the fluid flow driven by an external pressure gradient and buoyancy force in a porous vertical channel. In particular, the influence of anisotropy (permeability as well as thermal diffusivity) on the shift of the neutral stability curve is discussed. The linearly varying wall temperature is studied under two different types of perturbations, namely zero temperature and zero heat flux. The Prandtl number Pr^*, Forchheimer number, heat capacity ratio σ, and porosity ϵ were kept constant throughout the paper, and were set to 1, 1, 1, and 0.9, respectively.

It has been demonstrated that mixed convection in a vertical porous channel is unstable in a large portion of an appropriate parameter space under which the following conclusions can be made. Fully developed flow is most unstable in a highly permeable (which is a consequence of very low value of K_1 or high value of Da^*) as well as in very low diffusivity medium. It was observed that a reduction of permeability in the main flow direction by one order (i.e., a reduction of Da^* from 10^{-2} to 10^{-3}) makes the system remain stable for $Ra < 770$, whereas the flow become unstable even for $Ra = 150$ when permeability in the streamwise direction is reduced by an order of 2 (i.e., when K_1 is increased from 0.1 to 10). Depending on the value of permeability ratio, the flow in an anisotropic medium may be both more ($K_1 < 1$) or less ($K_1 > 1$) stable than that in an isotropic one.

In contrast to the viscous fluid case and that of an isotropic porous medium, where only unicellular flow pattern occur, in the case of anisotropic porous media, the flow pattern appears as single cells as well as double cells. For higher values of modified Darcy numbers, production of kinetic energy due to the shear term dominates over the same due to the buoyant term, to balance the total dissipation of energy in

nearly the entire Re range. Furthermore, it was also found that the dissipation energy associated with the Brinkman term is more significant than that associated with the Darcy term. However, in the case of lower values of modified Darcy number, flow becomes more stable and the disturbance thermal buoyant energy dominates in the entire Re range. Simultaneously, the impact of the Brinkman term in dissipating the kinetic energy becomes negligible compared to that of the Darcy term. Thus, inclusion of the Brinkman term, the Forchheimer term, and the nonlinear convective term in the momentum equations is a function of the permeability of porous medium. For the parameter range of the present paper, transition of instability from one type to another takes place in a smooth manner, except when permeability ratio K_1 exceeds 6. Wave number experiences an abrupt jump for most of the parameter ranges studied when Reynolds number reaches a threshold value. Quantitatively, the Reynolds number threshold value depends on the input parameters and the specific boundary conditions. In all the cases studied, the disturbance flow moved upwards as alternative single or double cells. It is worth mentioning that, beyond a certain threshold value of Re, the type of boundary condition did not alter the stability characteristics of the system.

Obviously, it is interesting and important to investigate the effect of variation of other parameters such as porosity, heat capacity ratio, and the Forchheimer number on the stability characteristics in more detail. This problem is left for a future study.

ACKNOWLEDGMENT

[1] P. R. Dando, J. A. Hughes, Y. Leahy, S. J. Niven, L. J. Taylor, and C. Smith, "Gas venting rates from submarine hydrothermal areas around the island of Milos, Hellenic Volcanic Arc," Cont. Shelf. Res. **15**, 913 (1995).
[2] P. R. Dando, D. Stüben, and S. P. Varnavas, "Hydrothermalism in the Mediterranean Sea," Prog. Oceanogr. **44**, 333 (1999).
[3] N. G. Holm, A. G. Cairns-Smith, R. M. Daniel, J. P. Ferris, R. J.-C. Hennet, E. L. Shock, B. R. T. Simoneit, and H. Yanagawa, "Future research," in *Marine Hydrothermal Systems and the Origin of Life*, edited by N. G. Holm (Kluwer Academic, Dordrecht, 1992).

[4]G. F. Scheele and T. J. Hanratty, "Effect of natural convection on stability of flow in a vertical pipe," J. Fluid Mech. **14**, 244 (1962).

[5]G. A. Kemeny and E. V. Somers, "Combined free and forced convective flow in vertical circular tubes—experiments with water and oil," Trans. ASME, Ser. C: J. Heat Transfer **84**, 339 (1962).

[6]L. S. Yao, "Is a fully-developed and non-isothermal flow possible in a vertical pipe?" Int. J. Heat Mass Transf. **30**, 707 (1987).

[7]L. S. Yao, "Linear stability analysis for opposed mixed convection in a vertical pipe," Int. J. Heat Mass Transf. **30**, 810 (1987).

[8]Y. C. Su and J. N. Chung, "Linear stability analysis of mixed-convection flow in a vertical pipe," J. Fluid Mech. **422**, 141 (2000).

[9]L. S. Yao and B. B. Rogers, "The linear stability of mixed convection in a vertical annulus," J. Fluid Mech. **201**, 279 (1989).

[10]S. A. Suslov and S. Paolucci, "Stability of mixed-convection flow in a tall vertical channel under non-Boussinesq conditions," J. Fluid Mech. **302**, 91 (1995).

[11]Y. Chen and J. N. Chung, "The linear stability of mixed convection in a vertical channel flow," J. Fluid Mech. **325**, 29 (1996).

[12]M. Combarnous and P. Bia, "Combined free and forced convection in porous media," Soc. Pet. Eng. J. **11**, 399 (1971).

[13]P. Cheng, "Combined free and forced boundary layer flows about inclined surfaces in a porous medium," Int. J. Heat Mass Transf. **20**, 807 (1977).

[14]P. Cheng, "Similarity solutions for mixed convection from horizontal impermeable surfaces in saturated porous media," Int. J. Heat Mass Transf. **20**, 893 (1977).

[15]P. Cheng, "Convective heat transfer in porous layers by integral methods," Lett. Heat Mass Transfer **5**, 243 (1978).

[16]F. C. Lai, F. A. Kulacki, and V. Prasad, "Mixed convection in horizontal porous layers: Effects of thermal boundary conditions," ASME Heat Transfer Division **84**, 91 (1987).

[17]K. J. Renken and D. Poulikakos, "Mixed convection experiments about a horizontal isothermal surface embedded in a water-saturated packed bed of spheres," Int. J. Heat Mass Transf. **33**, 1370 (1990).

[18]V. Prasad, F. C. Lai, and F. A. Kulacki, "Mixed convection in horizontal porous layers heated from below," ASME J. Heat Transfer **110**, 395 (1988).

[19]G. Castinel and M. Combarnous, "Natural convection in an anisotropic porous layer," Int. Chem. Eng. **17**, 605 (1977).

[20]J. F. Epherre, "Criterion for the appearance of natural convection in an anisotropic porous layer," Int. Chem. Eng. **17**, 615 (1977).

[21]A. Khalili, I. S. Shivakumara, and M. Huettel, "Effects of throughflow and internal heat generation on convective instabilities in an anisotropic porous layer," J. Porous Media (to be published).

[22]P. A. Tyvand, "Heat dispersion effect on thermal convection in anisotropic porous media," J. Hydrol. **34**, 335 (1977).

[23]R. McKibbin and P. A. Tyvand, "Anisotropic modeling of thermal convection in multilayered porous media," J. Fluid Mech. **118**, 315 (1982).

[24]P. A. Tyvand and L. Storesletten, "Onset of convection in an anisotropic porous medium with oblique principal axes," J. Fluid Mech. **226**, 371 (1991).

[25]M. Kaviany, *Principles of Heat Transfer in Porous Media* (Springer, New York, 1995).

[26]D. A. Nield and A. Bejan, *Convection in Porous Media* (Springer, New York, 1999).

[27]R. A. Wooding, "Steady state free thermal convection of liquid in a saturated permeable medium," J. Fluid Mech. **2**, 273 (1957).

[28]R. C. Givler and S. A. Altobelli, "A determination of the effective viscosity for the Brinkman–Forchheimer flow model," J. Fluid Mech. **258**, 355 (1994).

[29]N. Martys, D. P. Bentz, and E. J. Garboczi, "Computer simulation study of the effective viscosity in Brinkman's equation," Phys. Fluids **6**, 1434 (1994).

[30]D. F. James and A. M. J. Davis, "Flow at the interface of a model fibrous porous medium," J. Fluid Mech. **426**, 47 (2001).

[31]K. Vafai, "Convective flow and heat transfer in variable-porosity media," J. Fluid Mech. **147**, 233 (1984).

[32]V. Prasad, F. A. Kulacki, and M. Keyhani, "Natural convection in porous media," J. Fluid Mech. **150**, 89 (1985).

[33]K. Vafai and R. Thiyagaraja, "Analysis of flow and heat transfer at the interface region of a porous medium," Int. J. Heat Mass Transf. **30**, 1391 (1987).

[34]G. Lauriat and V. Prasad, "Non-Darcian effects on natural convection in a vertical porous enclosure," Int. J. Heat Mass Transf. **32**, 2135 (1989).

[35]A. J. Basu and A. Khalili, "Computation of flow through fluid–sediment interface in a benthic chamber," Phys. Fluids **11**, 1395 (1999).

[36]S. Chandrasekhar, *Hydrodynamic and Hydromagnetic Stability* (Dover, New York, 1961).

[37]P. G. Drazin and W. H. Reid, *Hydrodynamic Stability* (Cambridge University Press, Cambridge, 1981).

[38]P. Huerre and M. Rossi, "Hydrodynamic instabilities in open flows," in *Hydrodynamics and Nonlinear Instabilities*, edited by C. Godréche and P. Manneville (Cambridge University Press, Cambridge, 1998).

[39]IMSL, International Mathematical and Statistical Library (1982).

[40]C. Moler and G. W. Stewart, "An algorithm for generalized matrix eigenvalue problems," SIAM (Soc. Ind. Appl. Math.) J. Numer. Anal. **10**, 241 (1973).